ISSN 1001-0742
CN 11-2629/X

2012
Volume 24
Number 7

JOURNAL OF

ENVIRONMENTAL SCIENCES

ELSEVIER
Science Press

Sponsored by
Research Center for Eco-Environmental Sciences
Chinese Academy of Sciences

JOURNAL OF ENVIRONMENTAL SCIENCES

(http://www.jesc.ac.cn)

Aims and scope

Journal of Environmental Sciences is an international academic journal supervised by Research Center for Eco-Environmental Sciences, Chinese Academy of Sciences. The journal publishes original, peer-reviewed innovative research and valuable findings in environmental sciences. The types of articles published are research article, critical review, rapid communications, and special issues.

The scope of the journal embraces the treatment processes for natural groundwater, municipal, agricultural and industrial water and wastewaters; physical and chemical methods for limitation of pollutants emission into the atmospheric environment; chemical and biological and phytoremediation of contaminated soil; fate and transport of pollutants in environments; toxicological effects of terrorist chemical release on the natural environment and human health; development of environmental catalysts and materials.

For subscription to electronic edition

Elsevier is responsible for subscription of the journal. Please subscribe to the journal via http://www.elsevier.com/locate/jes.

For subscription to print edition

China: Please contact the customer service, Science Press, 16 Donghuangchenggen North Street, Beijing 100717, China. Tel: +86-10-64017032; E-mail: journal@mail.sciencep.com, or the local post office throughout China (domestic postcode: 2-580).

Outside China: Please order the journal from the Elsevier Customer Service Department at the Regional Sales Office nearest you.

Submission declaration

Submission of an article implies that the work described has not been published previously (except in the form of an abstract or as part of a published lecture or academic thesis), that it is not under consideration for publication elsewhere. The submission should be approved by all authors and tacitly or explicitly by the responsible authorities where the work was carried out. If the manuscript accepted, it will not be published elsewhere in the same form, in English or in any other language, including electronically without the written consent of the copyright-holder.

Submission declaration

Submission of the work described has not been published previously (except in the form of an abstract or as part of a published lecture or academic thesis), that it is not under consideration for publication elsewhere. The publication should be approved by all authors and tacitly or explicitly by the responsible authorities where the work was carried out. If the manuscript accepted, it will not be published elsewhere in the same form, in English or in any other language, including electronically without the written consent of the copyright-holder.

Editorial

Authors should submit manuscript online at http://www.jesc.ac.cn. In case of queries, please contact editorial office, Tel: +86-10-62920553, E-mail: jesc@263.net, jesc@rcees.ac.cn. Instruction to authors is available at http://www.jesc.ac.cn.

Copyright

ISSN 1001–0742 **Journal of Environmental Sciences** Vol. 24 No. 7 2012

CONTENTS

Serial parameter: CN 11-2629/X*1989*m*198*en*P*24*2012-7

Available online at www.sciencedirect.com
ScienceDirect
Journal of Environmental Sciences 2012, 24(7) 1197–1203
JOURNAL OF ENVIRONMENTAL SCIENCES
ISSN 1001-0742
CN 11-2629/X
www.jesc.ac.cn

Antimony(V) removal from water by iron-zirconium bimetal oxide: Performance and mechanism

Xuehua Li[1], Xiaomin Dou[1,2,*], Junqing Li[1,2]

1. Beijing Forestry University, Beijing 100083, China. E-mail: xhlibjfu@gmail.com
2. Beijing Key Laboratory for Source Control Technology of Water Pollution, Beijing Forestry University, Beijing 100083, China

Received 28 September 2011; revised 23 December 2011; accepted 31 December 2011

Abstract

A Fe-Zr binary oxide adsorbent has been successfully synthesized using a co-precipitation method. It showed a better performance for antimonate (Sb(V)) removal than zirconium oxide or amorphous ferric oxide. The experimental results showed that the Fe-Zr adsorbent has a capacity of 51 mg/g at an initial Sb(V) concentration of 10 mg/L at pH 7.0. Sb(V) adsorption on the Fe-Zr bimetal oxide is normally an endothermic reaction. Most of the Sb(V) adsorption took place within 3 hr and followed a pseudo second-order rate law. Co-existing anions such as SO_4^{2-}, NO_3^- and Cl^- had no considerable effects on the Sb(V) removal; PO_4^{3-} had an inhibitory effect to some extent at high concentration; while CO_3^{2-} and SiO_4^{4-} showed significant inhibitory effects when they existed in high concentrations. The mechanism of Sb(V) adsorption on the adsorbent was investigated using a combination of zeta potential measurements, XPS, Raman, FT-IR observations and SO_4^{2-} release determination. The ionic strength dependence and zeta potential measurements indicated that inner-sphere surface complexes were formed after Sb(V) adsorption. Raman and XPS observations demonstrated that both Fe-OH and Zr-OH sites at the surface of the Fe-Zr adsorbent play important roles in the Sb(V) adsorption. FT-IR characterization and SO_4^{2-} release determination further demonstrated that the exchange of SO_4^{2-} with Sb(V) also could promote the adsorption process. In conclusion, this adsorbent showed high potential for future application in Sb(V) removal from contaminated water.

Key words: antimony adsorption; iron-zirconium oxide; performance, mechanism

DOI: 10.1016/S1001-0742(11)60932-7

Introduction

Due to the widespread use of antimony-containing products, large amounts of Sb compounds are released into the water environment (Filella et al., 2002). Concentrations of Sb at the level of milligrams per liter are often found in or near smelters or facilities that manufacture ceramics or flame-retardant chemicals, while in unpolluted waters, concentrations of Sb are typically < 1 μg/L (Filella et al., 2002; Wilson et al., 2010). Seriously contaminated groundwaters containing Sb have been reported in China, India, New Zealand, Japan, etc (Filella et al., 2002; Wang et al., 2011; Wilson et al., 2004; Nakamura and Tokunaga, 1996; etc.).

Although there is still controversy concerning the details of its toxicity, antimony and its compounds have been considered as pollutants of priority interest by the United States Environmental Protection Agency (US EPA) and the European Environment Agency (EEA). The strict maximum contaminant level (MCL) is 6 μg/L in drinking water as set by US EPA, and is 5 μg/L set by the EEA and the Ministry of Health of China.

To minimize health risks, several technologies have been suggested for the purification of antimony-contaminated water, including coagulation-precipitation, membrane filtration and adsorption (Guo et al., 2009; Kang et al., 2000; Xi et al., 2010). Among these, adsorption has been considered an attractive method since it has been proved to be efficient, cost-effective and simple to perform. A variety of mineral sorbents including goethite, hematite, bauxite, kaolinite, bentonite and gibbsite have been extensively investigated for Sb removal (Xi et al., 2010, 2011; Rakshit et al., 2011; Mitsunobu et al., 2010). However, these studies have mostly focused on the interactions between antimony and naturally-occurring minerals from a geochemical point of view, aiming to demonstrate the distribution, transformation, transportation and fate of antimony in the natural environment. Besides the natural processes, heavy antimony pollution from mining processes, industrial accidents and shooting activities has frequently taken place and will probably occur again. Therefore, there has been an urgent demand for efficient engineering materials to mitigate antimony pollution, especially for emergency management of antimony accidents.

It is well known that iron oxides have strong binding affinity for Sb, and a variety of iron oxides have been reported to be effective for Sb removal. Apart from their inadequate adsorption capacities, characteristics such as

* Corresponding author. E-mail: douxiaomin@bjfu.edu.cn

availability, low cost and environmentally-friendly properties make them suitable candidates for antimony removal. To enhance the performance of iron oxides for the adsorption of anions, other elements (Mn, Al, Ce, Zr, etc.) have been incorporated and integrated with iron oxides to prepare bimetal oxides (Zhang et al., 2005, 2007, 2010; Masue et al., 2006; Zheng et al., 2009). Zirconium oxide has been well studied, since it has high resistance to acids, alkalis, oxidants and reductants. Zirconium oxides have been reported to be efficient for the removal of AsO_4^{3-} and PO_4^{3-} from water. Because P, As, and Sb are all group V elements, and elements in the same group tend to have similar chemical properties, it is expected that incorporation of zirconium into iron oxides would benefit from both the iron oxides and zirconium oxides.

In this study, a novel Fe-Zr bimetal oxide (Fe-Zr) adsorbent has been developed. The aim of the study was to assess the potential of such a composite adsorbent for the removal of antimonate from aqueous solutions by examining the effect of initial concentration, pH, temperature, ionic strength and coexisting anions. In addition, the mechanism of antimonate adsorption was investigated using a combination of zeta potential measurements, XPS, Raman, FT-IR observations and SO_4^{2-} release determinations.

1 Materials and methods

1.1 Materials

All chemicals were of analytical reagent grade. The Sb(V) stock solution was prepared by dissolving $NaSbO_3$ in deionized water. Sb-bearing solutions were freshly prepared by diluting the Sb(V) stock solution.

The Fe-Zr adsorbent was prepared at room temperature in the laboratory using a co-precipitation procedure. $Zr(SO_4)_2{\cdot}4H_2O$ (0.30 mol) and $FeSO_4{\cdot}7H_2O$ (0.15 mol) were dissolved in 1 L of deionized water. Under vigorous stirring, 1 mol/L NaOH was added at a rate of 12.5 mL/min to slowly raise the pH to the range 7.5 to 8.0. The pH was maintained in this range for 1 hr with continuous stirring and (if necessary) further addition of NaOH. Next, the suspension was allowed to settle, aged for 12 hr and then washed five times using deionized water. The suspension was filtered and dried at 65°C for 24 hr. The dry material was ground and sieved with a 100 mesh sieve and stored in a desiccator before use. Amorphous iron oxide (FeOOH) and zirconium oxide were prepared following a similar procedure.

1.2 Adsorbent characterization

The surface morphology of the materials was observed by FE-SEM using a HITACHI S-4500 (Japan). The specific surface area and pore volume of the Fe-Zr powder was determined by BET N_2 adsorption analysis using a Micromeritics ASAP2000 surface area analyzer (Norcross, USA). XRD patterns of the adsorbent were collected by an X'Pert PRO MPD diffractometer (PANalytical, the Netherlands) using Cu K_α radiation. Samples were scanned at a speed of 2°/min from 10° to 90°, at 40 kV and 40 mA. XPS spectra of the adsorbent before and after Sb(V) adsorption were recorded by a PHI Quantera spectrometer (USA). Raman spectra of samples were recorded on a 950 FT-Raman spectrometer (Nicolet, USA). The FT-IR spectra of samples were measured using a Spectrum GX spectrophotometer (PerkinElmer, USA) with a resolution of 2 cm^{-1}.

The zeta potential (ζ) of a 0.05 g/L Fe-Zr suspension was measured with 1 and 5 mg/L Sb(V), and without Sb(V) in the pH range 3 to 10 using a Zetasizer 2000 (Malvern Instruments Inc., UK), following a previously reported procedure (Jing et al., 2005).

1.3 Batch adsorption experiment

The adsorption isotherms were carried out by varying the initial concentrations of Sb(V) at a fixed adsorbent dose of 0.2 g/L, with a total volume of 100 mL in 250 mL glass vessels. The suspensions were continuously shaken at a speed of 160 r/min at 25 ± 1°C for 24 hr. The suspension pH was maintained at 7.0 ± 0.2 using 0.01 mol/L HCl and NaOH. For the Fe-Zr adsorbent, isotherm tests were also carried out at 15°C and 35°C. Kinetics experiments were performed to determine the reaction time to reach adsorption equilibrium. The Fe-Zr adsorbent was added to 1500 mL of Sb(V) solution to reach a dose of 0.2 g/L. The mixture was continuously stirred and the pH was adjusted and maintained at 7.0 ± 0.2 throughout the experiment. Approximately 4-mL aliquots were taken out at predetermined intervals and immediately filtered through a 0.45-μm membrane, and then analyzed.

The effect of ionic strength and solution pH on Sb(V) removal was determined in batch tests. A given volume of Sb(V) stock solution was added to vessels containing 100 mL NaCl solution, to make a concentration of 8 mg/L of Sb(V). The Fe-Zr adsorbent was added at a dose of 0.2 g/L, then the mixture was continuously shaken at 25 ± 1°C for 24 hr. The pH of the suspension was adjusted and maintained in the range of 3 to 11 during this period. In addition, the effects of coexisting anions (Cl^-, SO_4^{2-}, CO_3^{2-}, NO_3^-, PO_4^{3-}, SiO_4^{4-}, etc.) on Sb(V) adsorption were investigated without the addition of background electrolyte. Detailed results for the co-existing anions are provided in Table S1. The initial concentration of Sb(V) was fixed at 5 mg/L with a total volume of 100 mL, and a Fe-Zr dose of 0.2 g/L.

1.4 Analytical methods

The concentrations of residual Sb(V) were analyzed by a hydride generation-atom fluorescence spectrometer (HG-AFS, AF-610D2, Beijing Rayleigh Analytic Instrument Corporation, China) using a published method (Xi et al., 2010).

2 Results and discussion

2.1 Adsorbent characterization

The FE-SEM image of the sorbent is shown in Fig. S1a. It indicates that the surface of the sorbent is porous and shows nanograins with sizes ranging from 20 to 100 nm

aggregated and cohered on the surface. The BET analysis shows that the sorbent has a specific surface area of 121 m^2/g, which equates to a pore volume in excess of 0.37 cm^3/mg. To identify the phase structure of the sorbent, an XRD study was performed as shown in Fig. S1b. The results indicated a typical amorphous structure.

2.2 Adsorption isotherm

A comparison of the performance of Fe-Zr, FeOOH and zirconium oxide for Sb(V) removal is shown in Fig. 1. It was found that the Fe-Zr adsorbent had the highest adsorption capacity and the performance followed the order Fe-Zr > zirconium oxide > FeOOH. The Fe-Zr adsorbent performed well, as had been expected, by incorporation of Zr into the Fe oxides.

The adsorption isotherms were modeled using the Freundlich and Langmuir isotherm models (Fig. 1 and Table 1). It was found that both Freundlich and Langmuir models were suitable for describing the adsorption behavior of Sb(V). However, for the Fe-Zr adsorbent, the Langmuir model fitted the data much better, and the large values of $q_{m,L}$ and k_L demonstrated the high affinity of Sb for the Fe-Zr surface, implying a large number of available reactive sites for Sb adsorption (Table 1). The Langmuir isotherm model has also been used satisfactorily to well describe antimony adsorption on hydroxyapatite (Leyva et al., 2001), bentonite (Xi et al., 2011), kaolinite (Xi et al., 2010) and montmorillonite (Zhao et al., 2010).

In the present study, the Fe-Zr adsorbent showed a capacity of 51 mg/g at pH 7 with an initial Sb(V) concentration of 10 mg/L. This outperformed many other reported adsorbents for Sb(V), such as kaolinite at pH 6.0, 0.059 mg/g (Xi et al., 2010); bentonite at pH 6.0, 0.5 mg/g (Xi et al., 2011); goethite at pH 3.0, 17.9 mg/g (Leuz et al., 2006); and sodium montmorillonite, 40.75 mg/g (Zhao et al., 2010).

To further evaluate the thermodynamic feasibility and to confirm the nature of the adsorption process, the effect of temperature on the Sb(V) adsorption was investigated. As shown in Fig. 2, the capacity of Sb(V) increased with increasing temperature, which indicated an endothermic process. The thermodynamic nature of the adsorption was further defined by related parameters such as temperature (T, 15, 25, and 35°C), Gibbs free energy change (ΔG^0, –6.127, –4.503, and –2.636 kJ/mol at 15, 25 and 35°C, respectively), entropy change (ΔS^0 0.175 kJ/(mol·K)) and enthalpy change (ΔH^0 47.674 kJ/mol).

2.3 Adsorption kinetics

Figure 3 shows the time dependence of Sb(V) adsorption onto the Fe-Zr adsorbent. The equilibrium was reached within 1.5 and 3.0 hr, respectively, for the initial Sb(V) concentrations of 10 and 20 mg/L. Kinetic data for Sb(V) adsorption were fitted using the pseudo first- and second-order reaction rate models (Lagergren, 1898; Ho and McKay, 1999) according to Eqs. (1) and (2), respectively.

$$\log(q_e - q_t) = \log q_e - \frac{k_1}{2.303}t \quad (1)$$

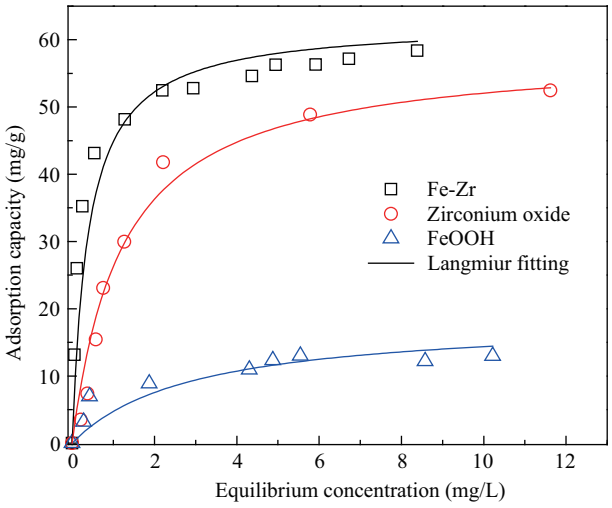

Fig. 1 Adsorption capacity comparison of Fe-Zr, Zr and Fe amorphous oxides. pH 7.0 ± 0.2; temperature 25 ± 1 °C; shaking time 24 hr; adsorbent dose 0.2 g/L; initial Sb(V) concentrations 0–25 mg/L.

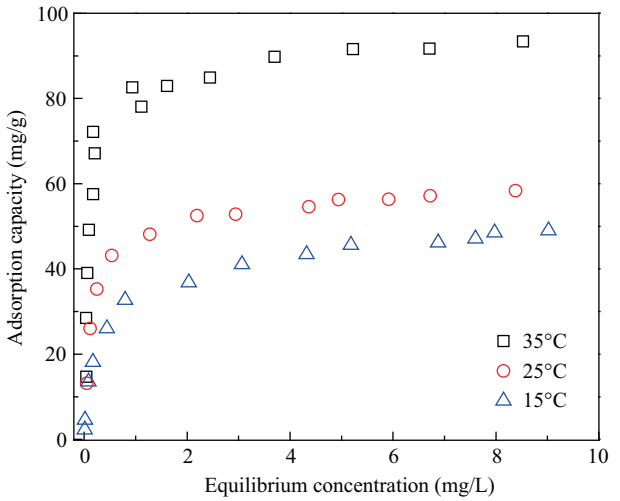

Fig. 2 Performance of Sb(V) removal by Fe-Zr oxide at different temperatures. pH 7.0 ± 0.2; shaking time 24 hr; adsorbent dose 0.2 g/L; initial Sb(V) concentrations 0–25 mg/L.

Table 1 Isotherm fitting for Sb(V) adsorption on the Fe-Zr binary oxide at various pH levels

	Equation	Parameters	Fe-Zr	Zirconium oxide	FeOOH
Langmuir	$q_e = \frac{q_{m,L} k_L C_e}{1+k_L C_e}$	$q_{m,L}$ (mg/g)	60.36	55.03	18.53
		k_L (L/mg)	3.483	1.013	0.343
		R^2	0.963	0.942	0.920
Freundlich	$q_e = k_F C_e^{1/n}$	k_F (g/(mg·L))	41.75	7.351	22.70
		$1/n$	0.186	0.272	0.391
		R^2	0.896	0.869	0.852

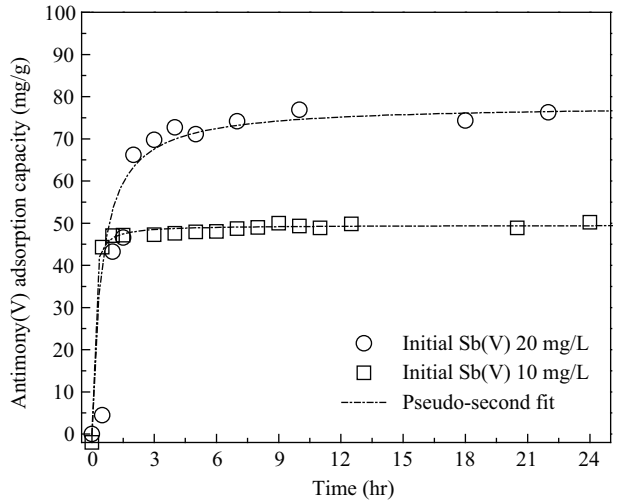

Fig. 3 Effect of contact time on Sb(V) adsorption on the Fe-Zr oxide. pH 7.0 ± 0.2; temperature 25 ± 1°C; adsorbent dose 0.2 g/L.

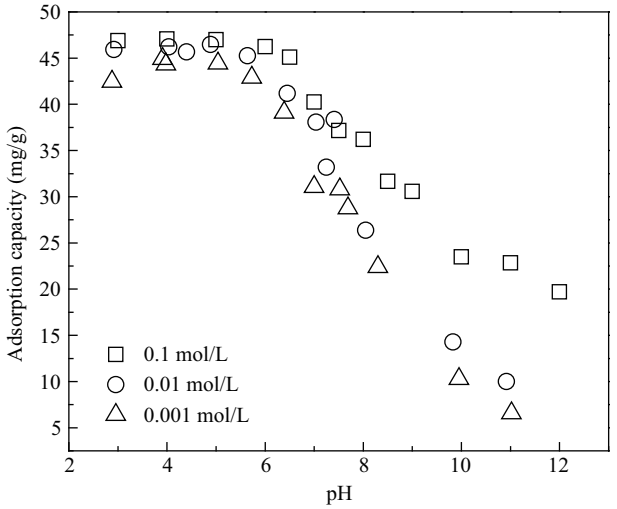

Fig. 4 Adsorption capacity as a function of pH under different ionic strength conditions. Temperature (25 ± 1)°C; shaking time 24 hr; adsorbent dose 0.2 g/L; initial Sb(V) concentration 10 mg/L.

$$\frac{t}{q_t} = \frac{1}{k_2 q_e^2} + \frac{1}{q_e} t \quad (2)$$

where, q_e (mg/g solid material) and q_t (mg/g solid material) are the amounts of adsorbed Sb at equilibrium and at time t (min), respectively. k_1 (min^{-1}) and k_2 (g/(mg·min)) are the equilibrium rate constants for pseudo first- and second-order sorption, respectively.

The calculated rate constants and related parameters are listed in Table 2. The high value of the determination coefficient (R^2) indicated that Sb(V) removal by the adsorbent followed a pseudo second-order rate law.

2.4 Effect of pH and ionic strength on Sb(V) adsorption on Fe-Zr

The effect of pH and ionic strength on Sb(V) adsorption on Fe-Zr is shown in Fig. 4. It can be seen that Sb(V) adsorption presented the typical "anions adsorption edge" shapes, showing decreased capacity with increasing pH values. The maximum capacity was observed below pH 5.5.

There was no significant shift in the position of the pH edge curves towards the alkaline region with ionic strength increasing from 0.001 to 0.01 mol/L over whole pH range and from 0.01 to 0.1 mol/L below pH 7.0; while a notable shift was observed from 0.01 to 0.1 mol/L above pH 7.0, showing higher adsorption performance with 0.1 mol/L than that with 0.01 mol/L. The effect of pH and ionic strength on the anion adsorption can also be used to infer the structure of the surface complexes formed. McBride et al. (1997) indicated that ions that form an outer-sphere surface complex show decreased adsorption with increasing ionic strength. Ions that form inner-sphere surface complexes show little ionic strength dependence or show increased adsorption with increasing ionic strength. The experimental results suggest that $Sb(OH)_6^-$ may form inner-sphere surface complexes at the surface of the adsorbent.

2.5 Effect of co-existing anions on Sb(V) adsorption on Fe-Zr

Usually, antimony-contaminated groundwater contains several other ions that may influence the adsorption performance. The effect of coexisting anions such as sulfate, chloride, nitrate, phosphate, bicarbonate and silicate on Sb(V) adsorption by the Fe-Zr adsorbent was investigated (Table S1). When presented in their naturally occurring concentrations, it was evident that SO_4^{2-}, NO_3^- and Cl^- had little effect on Sb(V) removal, while PO_4^{3-} had an inhibitory effect at high concentration (up to 10 mg/L). CO_3^{2-} and SiO_4^{4-} also showed significant inhibitory effects at high concentrations.

2.6 Adsorption mechanisms

2.6.1 Zeta potential measurement

The zeta potential of Fe-Zr with and without adsorbed Sb(V) as function of pH is shown in Fig. 5. It can be seen that the zeta potential and the isoelectric points (IEPs) of the suspension were shifted to more negative values with increasing Sb(V) concentrations. According to Goldberg and Johnston (2001), shifts in IEPs of minerals and reversals of the zeta potential with increasing sorbate concentration can be used as evidence of strong specific ion adsorption and inner-sphere surface complex formation. It is therefore supposed that specific adsorption of Sb(V) occurred and inner-sphere complexes were formed

Table 2 Kinetic parameters for Sb(V) adsorption on the Fe-Zr binary oxide under various initial concentrations

Initial concentration of Sb(V) (mg/L)	Pseudo first-order			Pseudo second-order		
	q_e (mg/g)	k_1 (1/hr)	R^2	q_e (mg/g)	k_2 (g/(mg·hr))	R^2
10	49.829	2.048	0.921	51.332	1.834	0.963
20	75.988	0.701	0.944	78.071	0.028	0.952

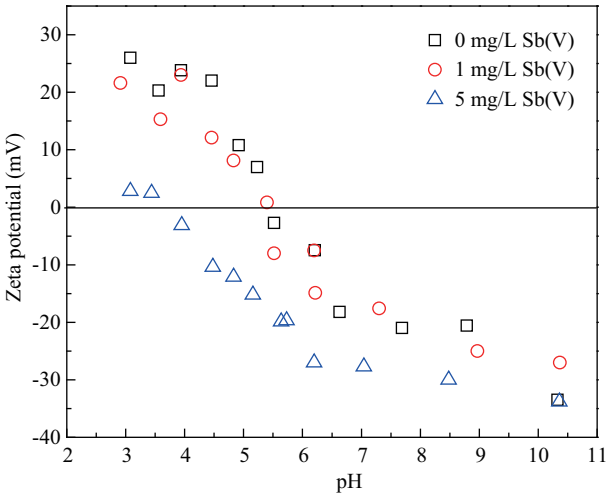

Fig. 5 Zeta potential of Fe-Zr oxide as function of pH at different Sb(V) concentrations.

on Fe-Zr, which is also in agreement with the investigation of ionic strength dependence described above (Fig. 4).

2.6.2 XPS characterization

XPS spectra of the Fe-Zr adsorbent before and after Sb(V) adsorption are presented in Fig. 6. It can be seen that Sb(V) was adsorbed onto the surface of the adsorbent (Fig. 6a), evidenced by the appearance of a $Sb3d_{3/2}$ peak in the narrow-scan spectrum of O1s+Sb3d (Fig. 6b). The peaks of Fe2p and Zr3d were clearly weakened (Fig. 6c–d), indicating a reaction of both Fe-OH and Zr-OH sites with Sb(V). In addition, the binding energies of O1s and Fe2p were shifted to lower values after Sb(V) adsorption. A core level shift of –0.6 and –0.4 eV for O1s + $Sb3d_{5/2}$ and $Fe2p_{3/2}$ was observed from the virgin adsorbent surface at 532.0 and 711.6 eV to the Sb(V)-adsorbed surface at 531.4 and 711.2 eV, respectively (Fig. 6b, c). The negative shifts of O1s and Fe2p were anticipated since Sb is more negative. The core level shifts reflected electron transfer in the valence band involving reactions between Sb and Fe/Zr. This indicated that both Fe-OH and Zr-OH sites played key roles in Sb(V) adsorption.

2.6.3 Raman characterization

The Raman spectra of the Fe-Zr adsorbent are shown in Fig. 7. For the sample before adsorption, the spectra mainly showed four bands at 245, 301, 390 and 998 cm^{-1}, which were typical signs of the existence of α-FeOOH (goethite). In addition, the bands 245 and 300 cm^{-1} were also observed from α-Fe_2O_3 and γ-Fe_2O_3, respectively (Oh et al., 1998). Since the adsorbent was prepared at low temperature without calcination, no obvious band for *m*-ZrO_2 (monoclinic phase) or *t*-ZrO_2 (tetragonal phase) was observed (Noda et al., 2007; Stefanc et al., 1999). After

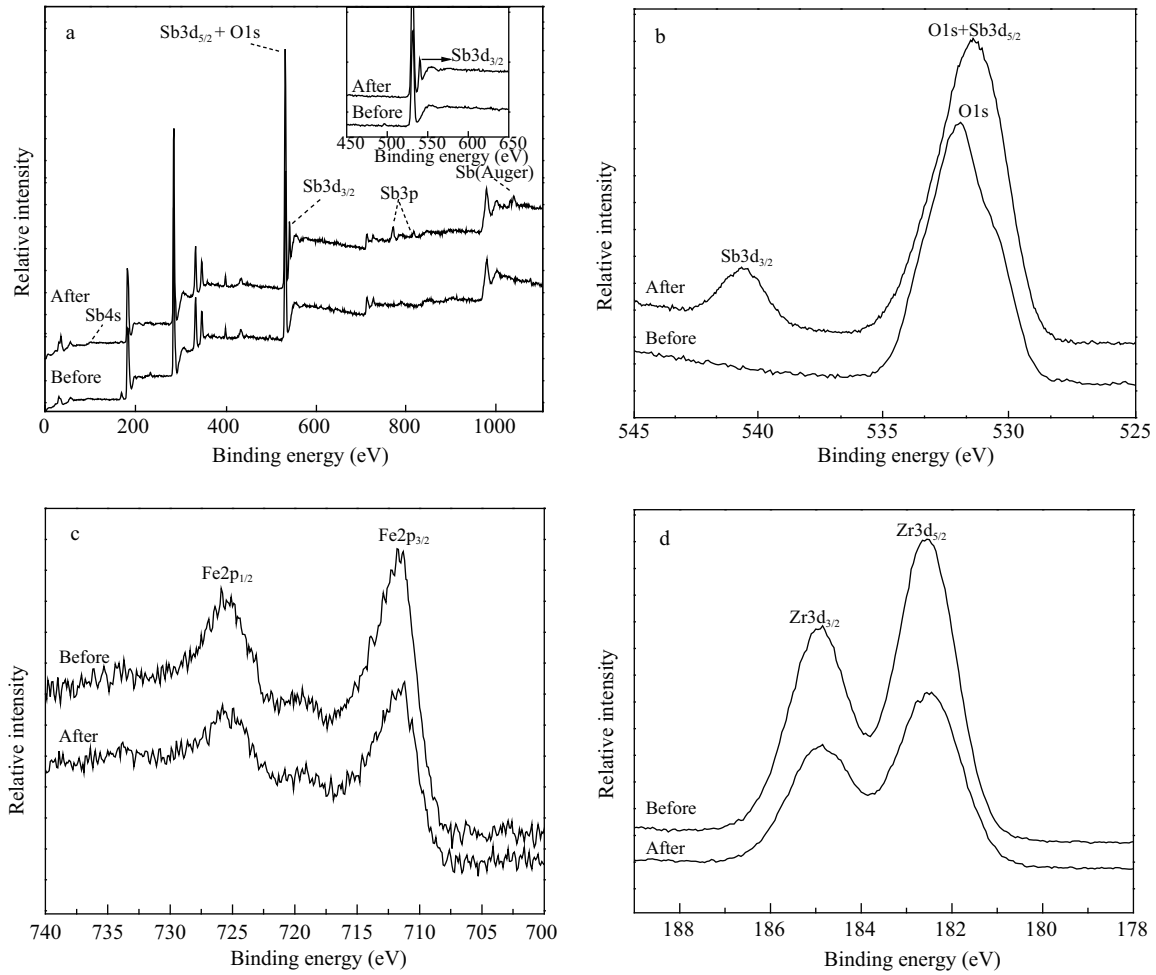

Fig. 6 XPS spectra of Fe-Zr oxide before and after reaction with Sb(V). (a) broad scan of samples; (b) narrow scan of O1s and Sb3d, (c) Fe2p and (d) Zr3d.

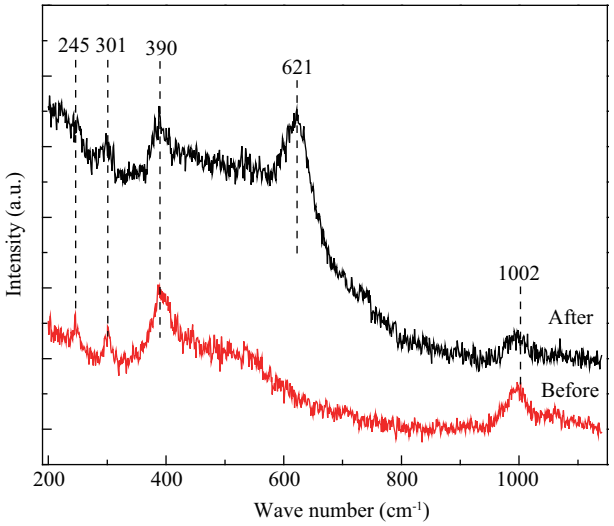

Fig. 7 Raman spectra of Fe-Zr oxide before and after Sb(V) adsorption at pH 7.0.

adsorption, a new band appeared at 621 cm^{-1}, which was assigned to the Sb-O symmetric stretch vibration (Rintoul et al., 2011), while bands at 245, 301, 390 and 998 cm^{-1} were all slightly weakened, indicating an interaction of the Sb(V) with the Fe-OH sites. The result agreed well with the XPS observations.

2.6.4 FT-IR characterization

FT-IR spectra of Fe-Zr adsorbent before and after adsorption are shown in Fig. 8. Broad absorption bands at 3000–3600 cm^{-1}, and a band at 1630 cm^{-1} were assigned to stretching modes of the OH bands of free water (surface adsorbed water), and the vibration of the H-O-H bond (Nakamoto, 2009). Bands at 1206, 1130, 1062 and 988 cm^{-1} were assigned to the asymmetric and symmetric S-O stretches of SO_4^{2-}, since $Zr(SO_4)_2{\cdot}4H_2O$ was used as the starting material and the final products contained sulfate. It was found the intensities of the SO_4^{2-} bands decreased gradually and disappeared with increasing initial Sb(V) concentrations from 0 to 40 mg/L. At an initial concentration of 40 mg/L, no new band appeared. Based on these facts, it is supposed that sulfate may be involved in the adsorption of Sb(V), and the content of sulfate in/on the adsorbent decreased with increasing Sb(V) concentration.

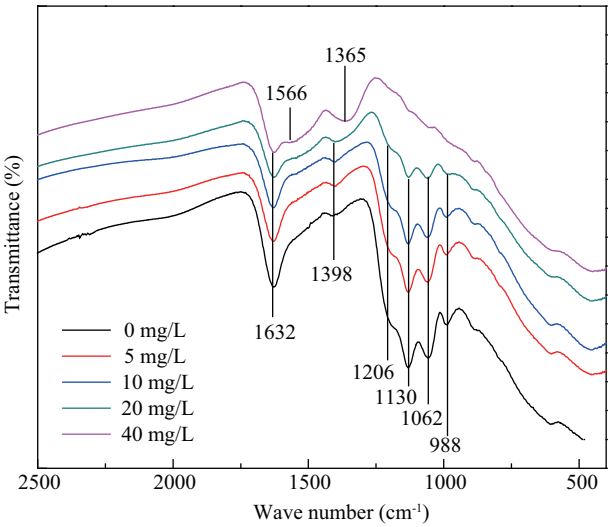

Fig. 8 FT-IR spectra of Fe-Zr oxide with Sb(V) adsorbed under different initial Sb(VI) concentrations.

2.6.5 Effect of Fe-Zr contained sulfate on Sb(V) adsorption

Since the FT-IR spectra indicated the involvement of sulfate in the adsorption of Sb(V), this observation was further investigated by a SO_4^{2-} release determination. The release of SO_4^{2-} during Sb(V) adsorption was determined over a wide range of initial Sb(V) concentrations (0–50 mg/L), as shown in Fig. S2. On the basis of the slope of the regression line, the Fe-Zr adsorbent released 0.33 mmol of SO_4^{2-} for every 1 mmol of Sb(V) sorbed. This shows that sulfate present in or on the adsorbent might be involved in the adsorption of Sb(V), which was in agreement with the results of the FT-IR observation. A similar result was also reported for As(V) adsorption on SO_4^{2-}-containing Fe-Ce bimetal oxide and schwertmannite (Fukushi et al., 2003; Zhang et al., 2010), in which 0.15–0.24 and 0.62 mmol SO_4^{2-}, respectively, were released for every 1 mmol of As(V). It was noticed that only 0.33 mmol of SO_4^{2-} was released in the present study, and therefore we infer that sulfate exchange is not likely to be the dominant mechanism for the adsorption of Sb(V).

3 Conclusions

A novel Fe-Zr bimetal oxide containing sulfate with a high capacity for Sb(V) adsorption was successfully prepared through a co-precipitation method. The adsorbent showed a capacity of 51 mg/g at pH 7.0 with an initial Sb(V) concentration of 10 mg/L, which is superior to that of FeOOH, zirconium oxide and many other reported adsorbents. Fe-Zr performed well under acid conditions, especially at pH values below 5.5. Kinetic results revealed that Sb(V) sorption onto Fe-Zr followed a pseudo second-order kinetic model. Except for CO_3^{2-}, SiO_4^{4-} and PO_4^{3-}, other coexisting anions such as Cl^-, NO_3^- and SO_4^{2-} had little effect on the Sb(V) adsorption at their typical concentrations in natural groundwater. The mechanism of Sb(V) adsorption on the adsorbent was thoroughly investigated using a combination of multiple techniques. The zeta potential measurement indicated the formation of inner-sphere surface complexes after Sb(V) adsorption as a result of interactions of both Fe-OH and Zr-OH sites with Sb(V), as indicated by the results of XPS and Raman spectra. In addition, SO_4^{2-} played a minor role in promoting Sb(V) adsorption, as demonstrated by FT-IR observations and the SO_4^{2-} release determination. In conclusion, the Fe-Zr adsorbent is a promising candidate for Sb(V) removal from contaminated water.

Acknowledgments

This work was supported by the Fundamental Research Funds for the Central Universities (No. YX-2010-33), the Major Projects on Control and Rectification of Water Body Pollution (No. 2008ZX07422-002-004) and the Beijing Nova Program (No. 2008A33).

Supporting material

Supplementary material associated with this article can be found in the online version.

References

Filella M, Belzile N, Chen Y W, 2002. Antimony in the environment: a review focused on natural waters: I. Occurrence. *Earth-Science Reviews*, 57(1-2): 125–176.

Fukushi K, Sato T, Yanase N, 2003. Solid-solution reactions in As(V) sorption by schwertmannite. *Environmental Science & Technology*, 37(16): 3581–3586.

Goldberg S, Johnston C T, 2001. Mechanisms of arsenic adsorption on amorphous oxides evaluated using macroscopic measurements, vibrational spectroscopy, and surface complexation modeling. *Journal of Colloid and Interface Science*, 234(1): 204–216.

Guo X, Wu Z, He M, 2009. Removal of antimony (V) and antimony (III) from drinking water by coagulation-flocculation-sedimentation (CFS). *Water Research*, 43(17): 4327–4335.

Ho Y S, McKay G, 1999. Pseudo-second order model for sorption processes. *Process Biochemistry*, 34(5): 451–465.

Jing C, Meng X, Liu S, Baidas S, Patraju R, Christodoulatos C, Korfiatis G P, 2005. Surface complexation of organic arsenic on nanocrystalline titanium oxide. *Journal of Colloid and Interface Science*, 290(1): 14–21.

Kang M, Kawasaki M, Tamada S, Kamei T, Magara Y, 2000. Effect of pH on the removal of arsenic and antimony using reverse osmosis membranes. *Desalination*, 131(1-3): 293–298.

Lagergren S, 1898. About the theory of so-called adsorption of soluble substances. *Kungliga Svenska Vetenskapsakademiens Handlingar*, 24(4): 1–39.

Leuz A K, Mönch H, Johnson C A, 2006. Sorption of Sb(III) and Sb(V) to goethite: influence on Sb(III) oxidation and mobilization. *Environmental Science & Technology*, 40(23): 7277–7282.

Leyva A G, Marrero J, Smichowski P, Cicerone D, 2001. Sorption of antimony onto hydroxyapatite. *Environmental Science & Technology*, 35(18): 3669–3675.

Masue Y, Loeppert R H, Kramer T A, 2006. Arsenate and arsenite adsorption and desorption behavior on coprecipitated aluminum: iron hydroxides. *Environmental Science & Technology*, 41(3): 837–843.

McBride M B, 1997. A critique of diffuse double layer models applied to colloid and surface chemistry. *Clays and Clay Minerals*, 45(4): 598–608.

Mitsunobu S, Takahashi Y, Terada Y, Sakata M, 2010. Antimony(V) incorporation into synthetic ferrihydrite, goethite, and natural iron oxyhydroxides. *Environmental Science & Technology*, 44(10): 3712–3718.

Nakamoto K, 2009 Infrared and Raman Spectra of Inorganic and Coordination Compounds (6th ed.). John Wiley, New York.

Nakamura Y, Tokunaga T, 1996. Antimony in the aquatic environment in north Kyushu district of Japan. *Water Science and Technology*, 34(7-8): 133–136.

Noda L K, Gonçalves N S, de Borba S M, Silveira J A, 2007. Raman spectroscopy and thermal analysis of sulfated ZrO_2 prepared by two synthesis routes. *Vibrational Spectroscopy*, 44(1): 101–107.

Oh S, Cook D C, Townsend H E, 1998. Characterization of iron oxides commonly formed as corrosion products on steel. *Hyperfine Interactions*, 112(1): 59–66.

Rakshit S, Sarkar D, Punamiya P, Datta R, 2011. Antimony sorption at gibbsite-water interface. *Chemosphere*, 84(4): 480–483.

Rintoul L, Bahfenne S, Frost R L, 2011. Single-crystal Raman spectroscopy of brandholzite $Mg[Sb(OH)_6]_26H_2O$ and bottinoite $Ni[Sb(OH)_6]_26H_2O$ and the polycrystalline Raman spectrum of mopungite $Na[Sb(OH)_6]$. *Journal of Raman Spectroscopy*, 42(5): 1147–1153.

Štefanć I I, Musić S, Štefanić G, Gajović A, 1999. Thermal behavior of ZrO_2 precursors obtained by sol-gel processing. *Journal of Molecular Structure*, 480-481: 621–625.

Wang X, He M, Xi J, Lu X, 2011. Antimony distribution and mobility in rivers around the world's largest antimony mine of Xikuangshan, Hunan Province, China. *Microchemical Journal*, 97(1): 4–11.

Wilson N J, Craw D, Hunter K, 2004. Antimony distribution and environmental mobility at an historic antimony smelter site, New Zealand. *Environmental Pollution*, 129(2): 257–266.

Wilson S C, Lockwood P V, Ashley P M, Tighe M, 2010. The chemistry and behaviour of antimony in the soil environment with comparisons to arsenic: a critical review. *Environmental Pollution*, 158(5): 1169–1181.

Xi J, He M, Lin C, 2010. Adsorption of antimony(V) on kaolinite as a function of pH, ionic strength and humic acid. *Environmental Earth Sciences*, 60(4): 715–722.

Xi J, He M, Lin C, 2011. Adsorption of antimony(III) and antimony(V) on bentonite: Kinetics, thermodynamics and anion competition. *Microchemical Journal*, 97(1): 85–91.

Zhang G S, Qu J H, Liu H J, Liu R P, Li G T, 2007. Removal mechanism of As(III) by a novel femn binary oxide adsorbent: oxidation and sorption. *Environmental Science & Technology*, 41(13): 4613–4619.

Zhang Y, Dou X M, Yang M, He H, Jing C Y, Wu Z Y, 2010. Removal of arsenate from water by using an Fe-Ce oxide adsorbent: Effects of coexistent fluoride and phosphate. *Journal of Hazardous Materials*, 179(1-3): 208–214.

Zhang Y, Yang M, Dou X, He H, Wang D, 2005. Arsenate adsorption on an Fe-Ce bimetal oxide adsorbent: role of surface properties. *Environmental Science & Technology*, 39(18): 7246–7253.

Zhao Z L, Wang X Q, Zhao C A, Zhu X G, Du S Y, 2010. Adsorption and desorption of antimony acetate on sodium montmorillonite. *Journal of Colloid and Interface Science*, 345(2): 154–159.

Zheng Y M, Lim S F, Chen J P, 2009. Preparation and characterization of zirconium-based magnetic sorbent for arsenate removal. *Journal of Colloid and Interface Science*, 338(1): 22–29.

Supporting materials

Effect of co-existing anions on Sb(V) adsorption

According to naturally occurring concentration ranges of anions in groundwater (Younger, 2007), co-existing anions were spiked into Sb(V) solution at three concentration levels to evaluate their effects on Sb(V) adsorption (Table S1). In the investigated conditions, it was seen that co-existing SO_4^{2-}, NO_3^- and Cl^- had no obvious inhibition effects on Sb(V) removal, while PO_4^{3-} has slight inhibition effecs and CO_3^{2-} and SiO_4^{4-} produced considerable inhibition effects at high concentrations.

Table A1 Effect of coexisting ion on Sb(V) adsorption

	Coexisting ion	Sb(V) removal		Coexisting ion	Sb(V) removal
SO_4^{2-} (mg/L)	100	94.20%	PO_4^{3-} (mg/L)	2	96.30%
	300	94.70%		5	92.20%
	500	94.80%		10	84.10%
NO_3^- (mg/L)	10	97.60%	CO_3^{2-} (mg/L)	50	86.80%
	30	97.20%		100	78.10%
	60	97.40%		200	58.50%
Cl^- (mg/L)	100	98.40%	SiO_4^{4-} (mg/L)	10	95.40%
	300	98.00%		20	70.40%
	500	96.20%		30	50.50%

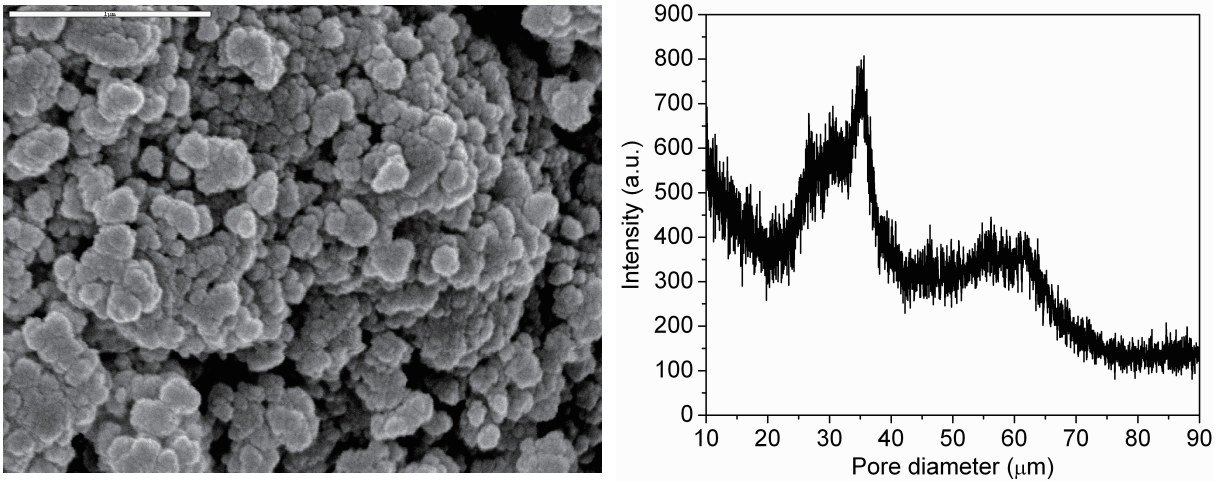

Fig. S1 FE-SEM image (a) and XRD pattern (b) of Fe-Zr binary oxide.

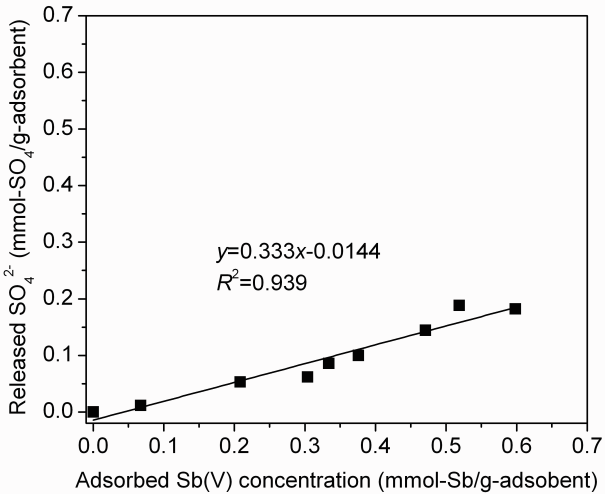

Fig. S2 Relationship between released SO_4^{2-} and adsorbed Sb(V). pH 5.0, initial Sb(V) concentration 0–16 mg/L.

JOURNAL OF ENVIRONMENTAL SCIENCES

Journal of Environmental Sciences (Established in 1989)
Vol. 24 No. 7 2012

Supervised by	Chinese Academy of Sciences	**Published by**	Science Press, Beijing, China
Sponsored by	Research Center for Eco-Environmental		Elsevier Limited, The Netherlands
	Sciences, Chinese Academy of Sciences	**Distributed by**	
Edited by	Editorial Office of Journal of	Domestic	Science Press, 16 Donghuangchenggen
	Environmental Sciences (JES)		North Street, Beijing 100717, China
	P. O. Box 2871, Beijing 100085, China		Local Post Offices through China
	Tel: 86-10-62920553; http://www.jesc.ac.cn	Foreign	Elsevier Limited
	E-mail: jesc@263.net, jesc@rcees.ac.cn		http://www.elsevier.com/locate/jes
Editor-in-chief	Hongxiao Tang	**Printed by**	Beijing Beilin Printing House, 100083, China

CN 11-2629/X **Domestic postcode: 2-580** **Domestic price per issue RMB ¥ 110.00**

ISSN 1001-0742